THE JOURNAL OF PHYSICAL CHEMISTRY A

pubs.acs.org/JPCA Article

Cation–π Complexes of Silver Studied with Photodissociation and Velocity-Map Imaging

Brandon M. Rittgers, Daniel Leicht, and Michael A. Duncan*

Cite This: J. Phys. Chem. A 2020, 124, 9166–9176 Read Online

ACCESS | Metrics & More | Article Recommendations | Supporting Information

ABSTRACT: Ag^+(aromatic) ion–molecule complexes of benzene, toluene, or furan are generated in the gas phase by laser vaporization in a supersonic expansion. These ions are mass selected in a time-of-flight spectrometer and studied with ultraviolet laser photodissociation and photofragment imaging. UV laser excitation results in dissociative charge transfer (DCT) for these ions, producing neutral silver atom and the respective aromatic cation as the photofragments. Velocity-map imaging and slice imaging techniques are employed to investigate the kinetic energy release in these photodissociation processes. In each case, DCT produces significant kinetic energy, and evidence is also found for excitation of the internal rovibrational degrees of freedom for the molecular cations. Analysis of the kinetic energy release together with the known ionization energies of silver and the molecular ligands provides new information on the cation–π bond energies.

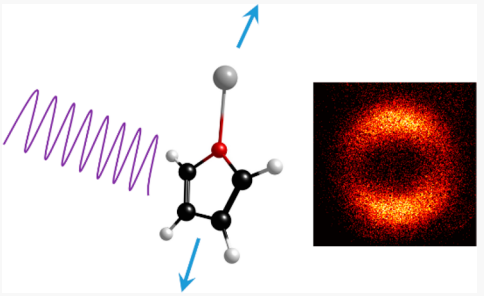

I. INTRODUCTION

Photoinduced charge transfer plays a pivotal role in photochemistry and energy transfer processes throughout chemistry and biology, lying at the heart of photosynthesis and solar energy generation.[1−6] These processes are well-documented in the spectroscopy and photochemistry of many inorganic or organometallic complexes.[7−10] Photoinduced charge transfer has also been observed for gas-phase molecular ions in mass spectrometry. Bowers and co-workers employed mass-analyzed ion kinetic energy spectroscopy to study dissociative charge transfer (DCT) processes in the visible spectra of atmospheric ion–molecule complexes.[11−13] Our lab has shown that similar DCT processes are prominent in the photodissociation of gas-phase metal ion–organic complexes of benzene or acetone.[14−17] Similar observations on other metal ion–organic species have been made by the groups of Kleiber and co-workers[18,19] and that of Yeh and co-workers.[20−24] Charge transfer is possible in these systems because of the relatively low ionization energies of aromatic molecules (8–10 eV), which are close to the ionization energies of metal atoms (6–9 eV). More recently, we have applied the technique of photofragment imaging to explore the kinetic energy release and energetics in such photodissociation processes.[25] These methods provide direct access to the energetics of cation–π interactions. In the present work, we apply these methods to investigate the Ag^+(benzene), Ag^+(toluene), and Ag^+(furan) complexes.

Metal ion–aromatic complexes are ubiquitous in organometallic chemistry, providing classic examples of cation–π interactions.[26−29] These complexes have also been well-studied in mass spectrometry, and their interactions have been investigated extensively with theory.[30−43] Because the ionization energies of most metal atoms are lower than those of ligands such as benzene, the charge in such metal–ligand ions resides on the metal in the ground electronic state. This has been demonstrated in several laboratories with collision-induced-dissociation (CID) experiments, which produce the metal cation as the only dissociation product.[33,35,38,41] With proper analysis, the thresholds for CID processes provide the bond energies for these complexes. For Ag^+(benzene), for example, the bond energy determined from CID by Chen and Armentrout was 37.4 kcal/mol.[33]

Excited electronic states for metal cation–molecular complexes correlate asymptotically to the excited atomic states of the metal cation and/or the excited states of the molecule. Electronic spectroscopy in the region of low-lying metal–cation electronic states has been studied for several cation–molecular complexes, allowing the structures of these complexes to be determined.[44−50] Additionally, cation–molecular complexes can possess "charge transfer" (CT) excited states whose asymptote correlates to the *neutral* metal and the aromatic *cation*. These states lie higher in energy than the ground state because of the difference in ionization potentials between the metal atom and ligands like benzene.[14−24] Because many transition metals have ionization energies in the 7–8 eV range, and the ionization energy of

Received: September 17, 2020
Revised: October 19, 2020
Published: October 26, 2020

https://dx.doi.org/10.1021/acs.jpca.0c08498
J. Phys. Chem. A 2020, 124, 9166–9176

benzene is 9.24 eV,[51] the charge transfer asymptote lies in the 1−2 eV range for metal ion−benzene complexes. Charge transfer transitions are therefore a general characteristic of the low-lying excited states of these systems. However, complexes of metal ions with no low-lying atomic-based excited states such as Ag^+ (the first excited $4d^9 5s^1$ state lies at 4.86 eV)[52] and no low-lying molecular-based states (e.g., benzene, first excited $\pi-\pi^*$ state at 262.6 nm (4.72 eV);[53] toluene, first excited state at 266.8 nm (4.65 eV);[54] furan, first excited state at 205.3 nm (6.04 eV)[55]) have *only* the charge transfer state at low energy. Excitation at low energy is therefore likely to excite the CT transition. This can be recognized in a photodissociation experiment by the production of the molecular cation as the photofragmentation product instead of the atomic metal cation.[14−24]

Photoinduced charge transfer dissociation has been observed previously for a variety of transition metal−aromatics using fixed-frequency dissociation in the near-UV wavelength region and detecting the aromatic cation as the photoproduct.[14−24] In some cases, the excitation spectra of the organic cation products were measured, and the threshold energies for DCT were documented.[15,18,19,21−23] Using this threshold energy, and the known ionization potentials for the metal ion and the aromatic molecules, an upper limit could be established for the cation−π bond energy via the expression

$$D_0''(M^+-L) \leq h\nu_0 - \Delta IP$$

where D_0'' is the cation−π bond energy, $h\nu_0$ is the photon energy at the threshold, and ΔIP is the ionization potential difference between the metal atom and the organic molecule. We used this threshold spectroscopy method previously to derive a bond energy for the Ag^+(benzene) complex,[15] and Yeh and co-workers used this method to derive a value for Ag^+(furan).[22,23] In recent work, our group has applied photofragment velocity-map imaging to this process, which determines the kinetic energy release in the aromatic cation following the DCT process.[25] A similar energetic cycle using the kinetic energy release provides the cation−π bond energy without the necessity of scanning the excitation spectrum:

$$D_0''(M^+-L) \leq h\nu_{CT} - (KER + \Delta IP)$$

where $h\nu_{CT}$ is the photon energy used for photodissociation, KER is the measured kinetic energy release, and the difference between these two quantities should be equivalent to $h\nu_0$ except for the effects of the Franck−Condon factors of the vertical transition in obscuring the adiabatic threshold. Our initial work investigated the Ag^+(benzene) ion with selected excitation energies in the UV.[25] Here, we apply this methodology to further investigate Ag^+(benzene) and for the first imaging measurements on Ag^+(toluene) and Ag^+(furan). These silver cation complexes are particularly convenient for these studies because of their relatively simple electronic structure resulting from the closed-shell d^{10} configuration of Ag^+.

II. METHODS

II.a. Experimental Section. Silver cation−π complexes were produced by laser vaporization at 355 nm (Continuum SureLite SL-10 Nd:YAG laser) using the so-called "cutaway" source configuration[56] and cooled in a supersonic expansion of argon. Benzene, toluene, or furan was entrained into the argon expansion gas using its ambient vapor above liquid samples at room temperature. The desired ions were extracted orthogonal to the molecular beam axis and mass selected using pulsed deflection plates for photodissociation in a reflectron time-of-flight spectrometer.[57,58] The configuration of the instrument can be adjusted to allow time-of-flight mass analysis of the photofragments in the reflected ion beam or to detect kinetic energy release via velocity-map imaging (VMI) of the transmitted ion beam. The selected-ion velocity-map imaging (SI-VMI) instrument has been described previously.[25] A figure of it is reproduced as Figure S1 (reproduced from ref 25; copyright 2015 American Chemical Society). For VMI experiments, the reflectron grids are grounded to transmit selected ions into the collinear imaging flight tube, where they are decelerated before photoexcitation. The photodissociation laser used for imaging is either a Nd:YAG (Spectra Physics GCR-170) or a Nd:YAG-pumped dye laser (Spectra Physics PDL-2). Photofragment ions are reaccelerated using a series of electrostatic lenses designed for velocity-map imaging[59−63] and detected using the DC-slice imaging technique.[64] To achieve slicing, the dual MCP/P-47 phosphor detector (Beam Imaging Solutions BOS-75) is activated in a narrow time window with a fast rise-time high voltage pulser (DEI PVX-4140), allowing fragment ions in the central ∼90 ns of the arrival-time distribution to be detected. The slicing method throws away 90% or more of the signal, but it allows the kinetic energy distribution of the image to be analyzed without extensive processing. Images are collected using a CCD camera (Edmund Optics), averaging over several hundred thousand laser shots. Images are processed with the NuAcq and BasisFit software of Suits.[65] A photomultiplier tube also observes the phosphor screen to detect ion time-of-flight information and monitor intensities.

This SI-VMI instrument has similarities to other experiments described recently for photofragment imaging of mass-selected ions,[66−77] but it also has special features. The ions are not produced by photoionization, but instead grow directly in the laser vaporization process as they undergo cooling in a supersonic expansion. Argon is employed as the expansion gas instead of helium to promote more efficient internal cooling of the ions. Other ions made under these same conditions have been demonstrated to have rotational temperature in the 10−50 K range. Ions are extracted perpendicular to the molecular beam flow direction, but then fly in a collinear path through the time-of-flight spectrometer for mass selection before entering the imaging flight tube section. The flight path from the molecular beam to the imaging detector is about 3 m, with 1.5 m from the photodissociation point to the detector. The ion beam energy is adjustable to optimize spatial filling of the detector with the ion image. The instrument is calibrated with the photodissociation of Ar_2^+ measured under the same ion beam settings. Ar_2^+ has been studied extensively, and its bond energy is well-known.[78,79] Analysis of its photodissociation images show that our instrument has no VMI lens-induced image expansion under the present ion beam conditions.[79] The ions that are imaged are not state selected as they are in some imaging experiments employing resonant photoionization. Instead, the detected ions represent a distribution of species in all internal states populated in the photodissociation process, and therefore the image provides an overview of the dynamics.

II.b. Computational Section. Computations of the structures and bonding energetics of these complexes were conducted using density functional theory (DFT) with the

https://dx.doi.org/10.1021/acs.jpca.0c08498
J. Phys. Chem. A 2020, 124, 9166−9176

B3LYP and M06-L functionals using both the def2-TZVP and def2-QZVP basis sets. These computations employed the Gaussian 16 program package.[80]

III. RESULTS AND DISCUSSION

Laser vaporization of a silver rod in the "cutaway" configuration of the cluster source[56] produces primarily atomic silver ions and not silver atom clusters. In combination with molecular vapor added to the expansion gas, a variety of ion−molecule clusters of the form $Ag^+(L)_n$ are produced, where "L" indicates the molecular species. The plasma conditions for laser vaporization in this configuration are gentle and lead to the addition of intact molecules to the metal ion without any significant fragmentation.[56] We presented mass spectra of $Ag^+(benzene)_n$ complexes in our previous work.[25] Figures 1

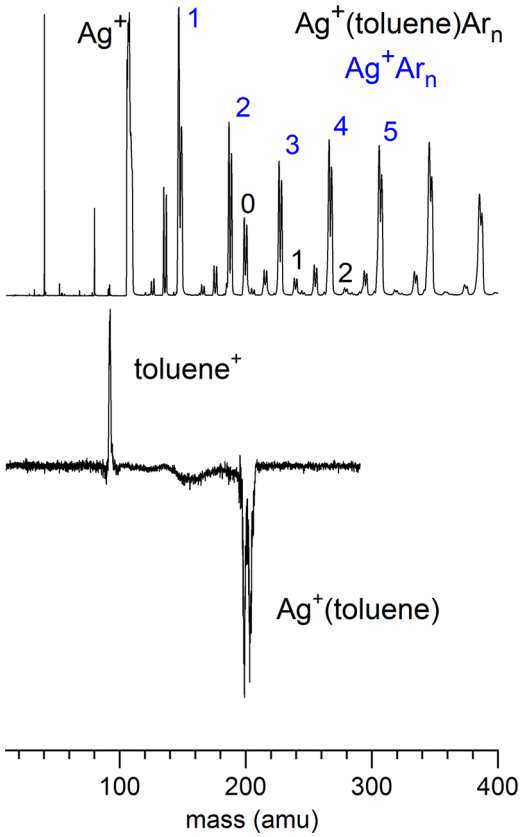

Figure 1. Mass spectrum (top) and 355 nm photodissociation mass spectrum (bottom) for the Ag^+(toluene) ion.

and 2 here show similar mass spectra for $Ag^+(toluene)_n$ and $Ag^+(furan)_n$ clusters. The mass spectrum for furan has ions corresponding to clusters containing multiple furan molecules, whereas the toluene mass spectrum has more argon complexes. This is because of the much higher vapor pressure of furan compared to that of toluene at room temperature.

The photodissociation mass spectra for Ag^+(toluene) and Ag^+(furan) at 355 nm are shown in the lower traces of Figures 1 and 2. The fragmentation spectra are collected in a difference mode of operation, in which the selected parent ion intensity before photoexcitation is subtracted from that of the diminished parent and fragment ion intensities produced with excitation, using multiple-shot averaging for each. The parent ion depletion then appears as a negative peak, and the fragment ion appears as a positive peak. In both cases, the only

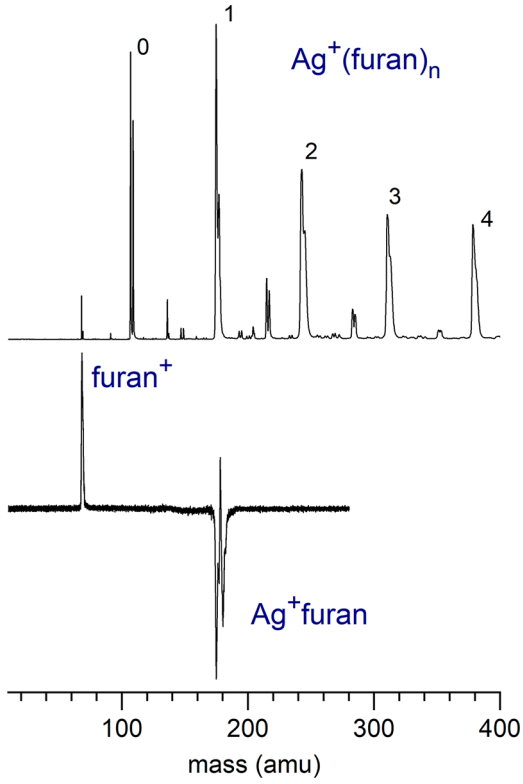

Figure 2. Mass spectrum (top) and 355 nm photodissociation mass spectrum (bottom) for the Ag^+(furan) ion.

fragment produced is the intact molecular cation and not the silver ion. This is evident because the parent ion depletion peaks have the isotopes of silver (107 and 109; 51.8 and 48.2% abundance) and the fragment ion peaks have only a single main isotope. Similar data was reported previously for Ag^+(benzene), which produces the benzene cation as the only photofragment.[14−16,25] This indicates that Ag^+(benzene), Ag^+(toluene), and Ag^+(furan) all undergo dissociative charge transfer at the 355 nm wavelength. This is consistent with previous work for Ag^+(benzene),[14−16,25] Ag^+(toluene),[15] and Ag^+(furan).[22,23] Similar DCT fragmentation is observed for these ions at the other UV wavelengths studied here (280 and 266 nm).

As discussed previously,[14−16,22−25] DCT is understandable for these ions because Ag^+ and the organics benzene, toluene and furan have no low energy excited states. The only electronic state at low energy is that corresponding to the charge-transfer excited state, with the Ag + L^+ asymptote. Figure 3 shows an example of the electronic states involved for the Ag^+(furan) complex, which is representative of the other complexes studied here. The ground state correlates to the Ag^+ + furan asymptote because the ionization potential of silver (7.576 eV) is lower than that of furan (8.886 eV).[81] Similar energetics apply for the complexes with benzene (IP = 9.244 eV)[82] and toluene (IP = 8.828 eV).[83] The excited states corresponding to excitation localized on the silver ion or the furan molecule lie at high energy, but the charge transfer excited state lies at an asymptotic energy corresponding to the ionization potential difference between silver and furan (ΔIP = 1.310 eV). The ground state is strongly bound by the electrostatic interaction between the silver cation and the polarizable molecule, whereas the excited state has the charge delocalized on the organic ion, which is polarizing the neutral

https://dx.doi.org/10.1021/acs.jpca.0c08498
J. Phys. Chem. A 2020, 124, 9166−9176

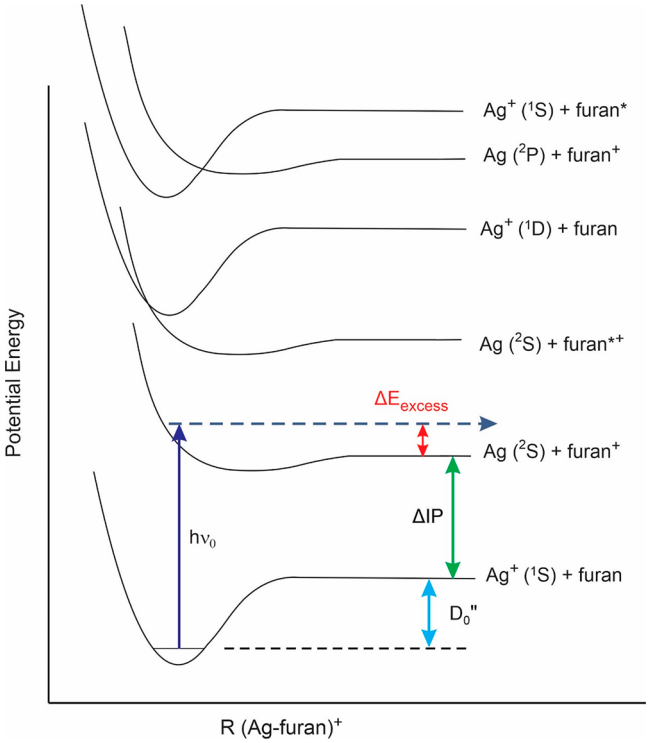

Figure 3. Schematic potential energy curves for the Ag^+(furan) complex demonstrating how dissociative charge transfer occurs and the source of the excess kinetic energy in the photofragments.

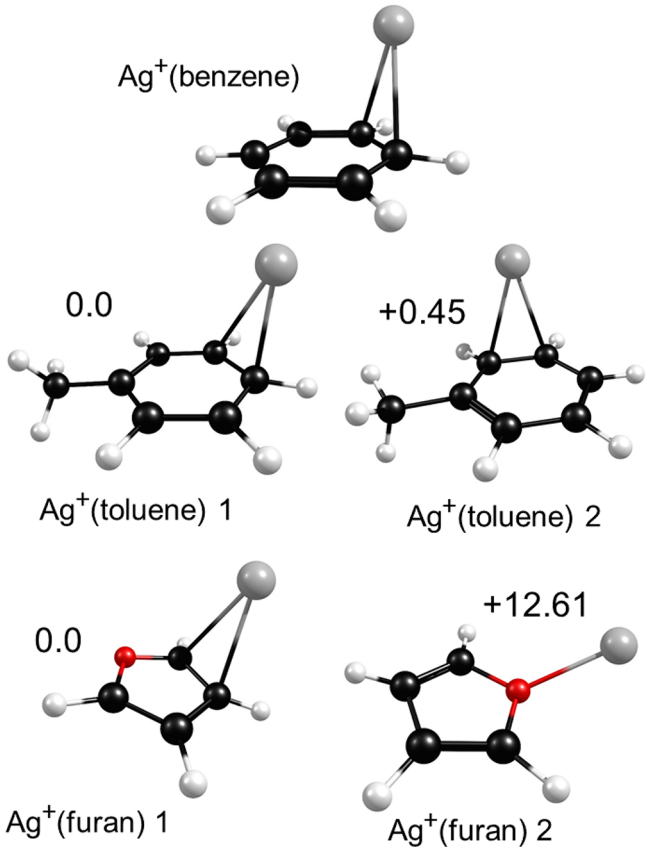

Figure 4. Structures resulting from computations for Ag^+(benzene), Ag^+(toluene), and Ag^+(furan) complexes. The toluene and furan complexes exhibit two isomers each. The relative energies of isomers are given at the M06-L/def2-QZVP level.

silver atom. The charge transfer excited state is therefore more weakly bonded than the ground state, and it is expected to have a longer Ag^+−L bond. The vertical excitation from the ground state therefore accesses the repulsive wall of the CT excited state, with the possible release of kinetic energy. The observation of the molecular cations as the only photofragments for these systems confirms that they all dissociate in the CT excited state. The imaging experiment here is designed to measure the excess kinetic energy released in the DCT process, if any.

To investigate the structures and energetics of these clusters, we have performed computational studies at the DFT/B3LYP and DFT/M06-L levels, each using the both the def2-TZVP and def2-QZVP basis sets. The full results of these computations are provided in the Supporting Information. Figure 4 shows the structures determined for these clusters, and Table 1 presents the Ag^+(L) binding energies for each of these complexes. Ag^+(benzene) has the structure reported previously,[25,38] with the metal ion attached above the midpoint of a C−C bond near the edge of the benzene ring. The metal−benzene bond energies computed here (36−38 kcal/mol) are similar to that from our previous work (37.3 kcal/mol)[25] and somewhat lower than the values obtained in older studies (40−44 kcal/mol).[32,38] Ag^+(toluene) binds in a similar way, but with the silver cation positioned asymmetrically above a C−C bond, lying closer to one carbon atom. The exact position of the silver varies with the different levels of theory. There are two kinds of binding sites: either opposite or adjacent to the methyl group. The most stable (isomer 1) is that with the metal binding remote from the methyl. The relative energies of these isomers vary slightly with the level of theory, but they are reflected in the difference in the Ag^+(toluene) binding energies. Therefore, isomer 1 is predicted to be 0.9 kcal/mol more stable than isomer 2 at the B3LYP/def2-TZVP level. The dissociation energies of these two isomers are almost the same (39−41 kcal/mol), and both are systematically higher by 2−3 kcal/mol than the values computed for Ag^+(benzene). Ag^+(furan) also has two isomers, with the structure having the metal ion over the adjacent C−C bond (isomer 1) lying at lower energy than one with it attached to the oxygen atom and slightly out of the plane of the aromatic system (isomer 2). Isomer 1 is predicted to be 12.3 kcal/mol more stable than isomer 2 at the B3LYP/def2-TZVP level. Consequently, it has a higher computed dissociation energy (36−38 kcal/mol) than isomer 2 (23−26 kcal/mol).

III.a. Ag^+(benzene) Imaging. Figure 5 shows the images obtained for the benzene cation photofragment from Ag^+(benzene) for excitation at 355, 280, and 266 nm. This ion was studied in our previous work with photodissociation at 355 and 266 nm;[25] new images presented here at these wavelengths are completely consistent with those measured previously. The left frames of Figure 5 show the raw images (no processing) of the benzene cation resulting from the photodissociation process, and the right frames show the total kinetic energy release profiles resulting from the analysis of these images. As shown in the images and the kinetic energy spectra, a wide range of KER values is produced in these DCT processes. As we discussed in our previous study,[25] this indicates that the benzene cation produced as a photofragment has significant internal energy in rotational and/or vibrational degrees of freedom resulting from the dissociation. This is

https://dx.doi.org/10.1021/acs.jpca.0c08498
J. Phys. Chem. A 2020, 124, 9166−9176

Table 1. Bond Dissociation Energies (in kcal/mol; ZPE Corrected) Resulting from Our Computations for Ag^+(benzene), Ag^+(furan), and Ag^+(toluene), Compared to the Upper Limits Derived Here for These Bond Energies and to the Results of Previous Theory

	B3LYP		M06L		
	def2-TZVP	def2-QZVP	def2-TZVP	def2-QZVP	comparison
Ag^+(benzene)	37.83	38.30	36.58	37.53	≤28.9 ± 3.2[a]
					≤30.0[b]
					≤32.8 ± 1.5[c]
					37.4 ± 1.7[d]
					35.4 ± 2.3[e]
					55 ± 5[f]
					44.2[g]
					40.0[h]
Ag^+(toluene)					≤35.9 ± 3.2[a]
					≤58 ± 5[f]
isomer 1	40.86	41.38	39.38	40.29	
isomer 2	40.03	40.55	38.92	39.84	
Ag^+(furan)					≤26.3 ± 3.2[a]
					≤28.1[i]
isomer 1	37.21	37.51	35.70	36.55	
isomer 2	24.95	25.64	22.66	23.94	

[a]Present experiments. [b]Tunable laser threshold spectroscopy (ref 15). [c]Previous imaging experiments (ref 25). [d]Collision-induced dissociation (ref 32). [e]Reanalysis of data in ref 32 (ref 25). [f]UV lamp photodissociation (ref 34). [g]MP2 theory (ref 38). [h]CCSD(T) theory (ref 38). [i]Tunable laser threshold spectroscopy (ref 22).

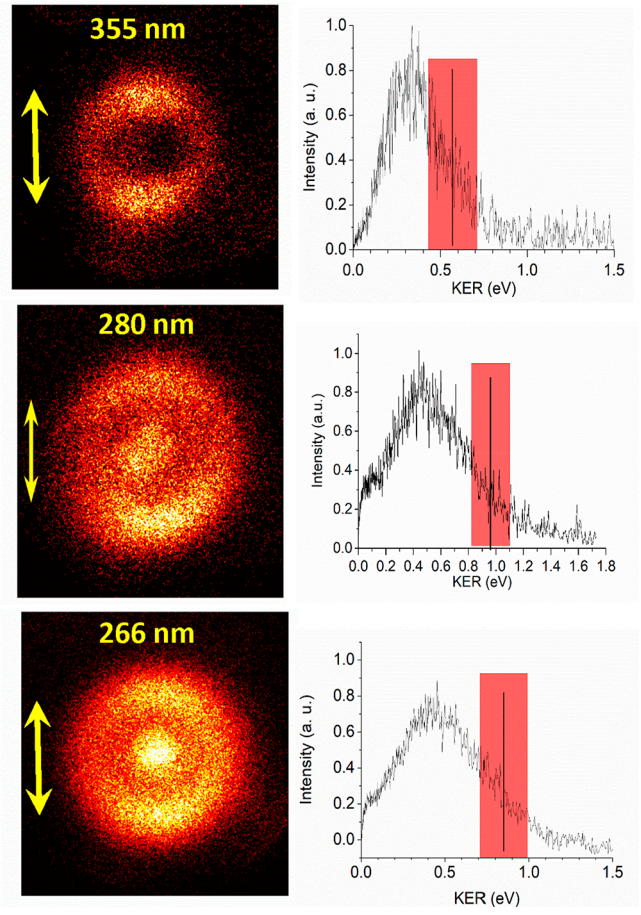

Figure 5. Photofragment images and kinetic energy spectra for Ag^+(benzene) at 355 (top), 280 (middle), and 266 nm (bottom). The yellow arrows in each frame indicate the laser polarization. The colored boxes indicate the maximum KER values and their uncertainties.

possible because the structure of the Ag^+(benzene) ion (Figure 4) has the silver in a low symmetry position above a C−C bond on the edge of the benzene ring, so that dissociation can lead to significant torque. Rotational excitation and/or vibrational excitation is therefore possible in the dissociation process. Internal vibrational excitation can also result from the vertical transition from the ground electronic state to the charge transfer excited state, determined by the Franck−Condon factors for the transition. The distribution of internal energies must be matched by a corresponding distribution of kinetic energies. As shown in Figure 5, the kinetic energy ranges from a maximum value of about 1 eV all the way down to zero, but the majority of the signal lies between 0.2 and 1.0 eV. This suggests that most of the fragment benzene ions produced have some significant kinetic energy, and very few have the excess energy of the dissociation deposited completely into the internal degrees of freedom. Images at different excitation wavelengths indicate somewhat similar behaviors. However, the 355 nm image has hardly any signal at its center, indicating very little near-zero KER and a greater tendency for translational excitation. The image at 266 nm has a much greater signal at its center, indicating a much greater amount of near-zero KER and more internal excitation.

The vertical yellow arrows in Figure 5 show the laser polarization used for the experiments. In the image at 355 nm, the signal is concentrated in north−south lobes along the direction of the laser polarization plane, with a partial node in the east−west direction. A fit of the angular distribution of the image results in a β parameter of 0.38. A similar angular distribution (β = 0.37) is observed for photodissociation of this ion at the 280 nm wavelength, and a more isotropic distribution (β = 0.17) is observed for photodissociation at 266 nm. These values are presented in Table 2. These β values are of course affected by the broad distribution of kinetic energies. The anisotropy is nearly the same for excitation at 355 and 280 nm, but at 266 nm the image is almost isotropic. This may be caused by different Franck−Condon factors for

https://dx.doi.org/10.1021/acs.jpca.0c08498
J. Phys. Chem. A 2020, 124, 9166−9176

Table 2. Ionization Energies, Measured Kinetic Energy Release, Anisotropy Parameters, and Derived Upper Limits to the Bond Energies for the Ag^+(aromatic) Complexes Studied Here

complex	ΔIP (eV)	λ_{Exc} (nm)	max KER (eV)	D_0'' limit (kcal/mol)	β
Ag^+(benzene)	1.668	355	0.57	28.9 ± 3.2	0.38
Ag^+(benzene)	1.668	280	0.96	41.6 ± 3.2	0.37
Ag^+(benzene)	1.668	266	0.85	49.4 ± 3.2	0.17
Ag^+(toluene)	1.252	355	0.68	35.9 ± 3.2	0.42
Ag^+(toluene)	1.252	266	0.86	58.8 ± 3.2	0.07
Ag^+(furan)	1.31	355	1.04	26.3 ± 3.2	1.17
Ag^+(furan)	1.31	266	0.86	57.4 ± 3.2	0.91

excitation at this higher energy, producing more vibrational excitation prior to separation of the fragments. It could also reflect some electronic mixing between the charge transfer state and the HOMO−LUMO excitation on the benzene, which in the isolated molecule occurs near 260 nm.[53] If the electronic transition moment for excitation of the benzene is different from that for the charge transfer, this would cause a more isotropic distribution. Predissociation involving such another state could cause rotation of the excited complex before its separation, washing out the initial polarization from the excitation.

Although there is significant internal excitation of the benzene in each of these spectra, the maximum kinetic energy values at the periphery of the images still provide useful information about the metal−ligand bond energy. Because we cannot guarantee that the maximum value detected is the full excess energy going into kinetic energy, this highest detected KER value represents a lower limit on the total excess energy. The shaded regions of the KER plots in Figure 5 show the maximum values derived from these data, and the widths of the boxes indicate the error bars, derived from the instrument resolution. The instrument resolution is derived from the width of the atomic ion image of Ar^+ from the photodissociation of Ar_2^+ measured in this instrument with the same ion beam energy. In that case, the photofragments are atomic and there is no possibility of internal excitation. Figure S2 provides a detailed explanation of how the maximum kinetic energy value is derived. We determine a baseline noise level for areas outside the image, and then we determine the threshold signal level rising above this on the high energy side of the KER curve. We set the upper limit of the instrument KER resolution width here, and we assign the threshold to be at the center of this width. For example, the maximum kinetic energy detected at the 280 nm CT wavelength is 0.96 ± 0.14 eV. Using the photon energy and the ionization potential difference between Ag (7.576 eV) and benzene (9.244 eV),[82] ΔIP = 1.668 eV, we derive an upper limit on the Ag^+(benzene) bond energy of 41.6 ± 3.2 kcal/mol. The main contribution to the error bars in this determination is the uncertainty in the measured KER value resulting from the instrument resolution, as the photon energy and ionization energies are known with much higher accuracy.

The maximum KER at the 280 nm dissociation wavelength can be compared to the values determined previously at the 355 and 266 nm wavelengths, which are presented in Table 2. As shown, the maximum amounts of kinetic energy detected are 0.57 and 0.85 eV at the 355 and 266 nm wavelengths. These values are slightly different from those which we reported previously for this system.[25] We have reproduced the images seen before, but we have improved our calibration and the method for determining the edge of the image, resulting in the slightly modified numbers. Our error bars have also been widened compared to the previous numbers. The higher KER at 280 nm compared to that at 355 nm reflects in part the higher excitation energy. The lower value at 266 nm makes sense in light of the significant change in image symmetry, probably reflecting some electronic state mixing and a greater fraction of internal excitation on the benzene cation.

All of these KER values result in different upper limits on the Ag^+(benzene) bond energy, but the tightest value is obtained at the lowest excitation energy at 355 nm. The 0.57 eV maximum KER value here cycles to an upper limit on the bond energy of 28.9 ± 3.2 kcal/mol. This number is lower than our previously reported value from imaging (32.8 ± 1.5 kcal/mol), resulting from the new calibration and more realistic error bars, as noted above. However, the value here is in good agreement with our previous result of 30.0 kcal/mol, derived by scanning a tunable laser and locating the threshold for the appearance of the charge transfer benzene cation fragment.[15] As discussed previously, all of these numbers are somewhat lower than the previous experimental result of Armentrout and co-workers using collision-induced dissociation (37.4 ± 1.7 kcal/mol)[33] and a revised value obtained more recently by reanalysis of the original data (35.4 ± 2.3 kcal/mol).[25] They are also lower than the results of our computational studies, as well as the results of previous computational work, as shown in Table 1. Previous computational studies found dissociation energies in the 34−44 kcal/mol range.[32,38]

III.b. Ag^+(toluene) Imaging. Figure 6 shows the photofragment images obtained for the toluene cation from the photodissociation of Ag^+(toluene) with excitation at 355 and 266 nm. The analyses of these images and their angular distribution fits are given in Figures S8−S11. In Figure 6, the image at 355 nm looks quite similar to that seen for Ag^+(benzene) at this same excitation energy, with polarized north−south lobes and only a small amount of signal near the

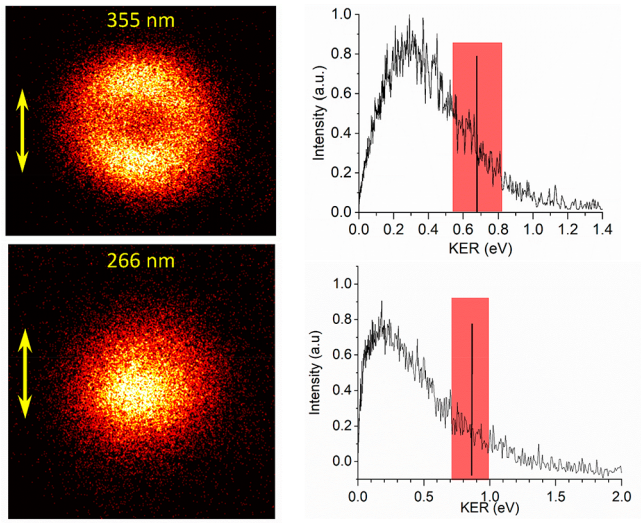

Figure 6. Photofragment images and kinetic energy spectra for Ag^+(toluene) at 355 (top) and 266 nm (bottom). The yellow arrows in each frame indicate the laser polarization. The colored boxes indicate the maximum KER values and their uncertainties.

https://dx.doi.org/10.1021/acs.jpca.0c08498
J. Phys. Chem. A 2020, 124, 9166−9176

center of the image corresponding to low KER values. The β parameter resulting from the fit of this image is 0.42, which is slightly more anisotropic than the corresponding silver−benzene image. The broad distribution of KER values can be attributed to factors similar to those for the Ag^+(benzene) complex, as theory shows that the structure of the complex has similar bonding with the metal asymmetrically positioned above C−C bonds on the edge of the ring in both of its isomers.

The image and angular distribution fit obtained for photodissociation at 266 nm are dramatically different from those at 355 nm, with a central bright spot trailing away gradually to higher energy and virtually no anisotropy (β = 0.07). This indicates that only a small fraction of the possible excess energy goes into KER and that much of the energy goes into the internal degrees of freedom of the toluene cation. As in the case of the Ag^+(benzene) complex, there are several possible reasons for the change in dynamics at the higher excitation energy. The most intriguing is the possibility of electronic state mixing. Neutral toluene has its first excited electronic state at lower energy than that of benzene, and this HOMO−LUMO excitation occurs at 266.8 nm.[54] This suggests that the charge transfer excitation and some excitation of the neutral toluene ligand might both occur at the 266 nm excitation wavelength. The dissociation which produces toluene cation, the measured fragment ion, must occur eventually on the charge transfer electronic state. But excitation into a state with mixed character, followed by predissociation, rotation of the parent, and/or significant loss of kinetic energy into the internal degrees of freedom before dissociation on the DCT potential would be consistent with the more isotropic KER distribution. Tunable laser excitation spectra in this region and in the region toward higher energy would be interesting to probe the extent of DCT and the possible changeover to the production of non-DCT Ag^+ fragment ions.

As we noted above for the Ag^+(benzene) complex, the maximum value of the KER can be used to set limits on the complex dissociation energy even if the dynamics cause efficient internal excitation of the departing organic cation. In the Ag^+(toluene) system, the maximum KER values for excitation at 355 and 266 nm are 0.68 and 0.86 eV, respectively. Again, the 355 nm data provides the tightest upper limit on the dissociation energy. Using the photon energy and the ionization potential difference between Ag (7.576 eV) and toluene (8.828 eV),[83] ΔIP = 1.252 eV, we derive an upper limit on the Ag^+(toluene) bond energy of 35.9 ± 3.2 kcal/mol. This compares to our computed values for the bond energy of 39−41 kcal/mol, which vary depending on the isomeric structure, as well as the functional and basis set, as shown in Table 1. As seen for the Ag^+(benzene) complex, the upper limit derived here is well below the bond energy predicted by theory for either isomer. In this case, the one previous experimental value is a much higher upper limit (≤58 kcal/mol)[34] and there are no previous computational values to compare to.

According to our computations and experiments, the bond energy for Ag^+(toluene) is greater than that for Ag^+(benzene). This is expected on the basis of previous work on transition-metal cation−arene complexes.[37] In a systematic study of many cation−arene complexes using the kinetic method, Schwarz and co-workers noted that electron-donating groups such as $-CH_3$ increased the cation−π bond energies.[37] This was attributed to increased π electron density in the ring system, which facilitates the cation−π interaction. However, the metals in that study were bound to the arenes in the sixfold symmetric site, whereas the silver ion here binds above the ring edge. It is not clear, therefore, that the same trend should be observed. In more recent work, Wheeler and co-workers have pointed out that local dipoles rather than shifts in aromatic electron density are responsible for the cation−π binding in substituted benzenes.[84,85] It seems clear that the Ag^+(toluene) binding is stronger than that of Ag^+(benzene), but the detailed explanation of this may require further computational work like that of Wheeler's to decompose the nature of the electrostatic interactions.

III.c. Ag^+(furan) Imaging. Figure 7 shows the images obtained for the furan cation photofragment from the photodissociation of Ag^+(furan) with excitation at 355 and 266 nm. The analysis of these images is presented in Figures S12−S15. In Figure 7, the image at 355 nm is more anisotropic (β = 1.17) than those for silver−benzene and silver−toluene, with more well-defined north−south lobes of intensity and less signal in the low KER area near the center of the image. The distribution of KER values is still somewhat broad, indicating some excitation of the internal degrees of freedom of the furan cation. The image at 266 nm is quite similar to that obtained at 355 nm, with a similar KER distribution and anisotropy (β = 0.91). In the case of furan, the first excited state of the ligand is at much higher energy than it is for either benzene or toluene, so the excitation here is likely hitting a state with pure charge transfer character.

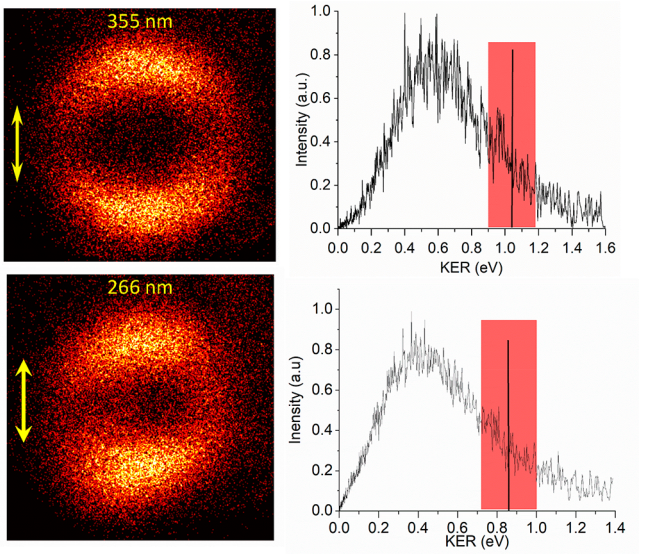

Figure 7. Photofragment images and kinetic energy spectra for Ag^+(furan) at 355 (top) and 266 nm (bottom). The yellow arrows in each frame indicate the laser polarization. The colored boxes indicate the maximum KER values and their uncertainties.

Following the same procedure outlined above, we can use the outside edges of the images in Figure 7 to obtain maximum KER values for these dissociation processes, and from those values determine upper limits on the dissociation energies. Using the photon energy and the ionization potential difference between Ag (7.576 eV) and furan (8.886 eV),[81] ΔIP = 1.310 eV, we derive upper limits on the Ag^+(furan) bond energy of 26.3 ± 3.2 and 57.4 ± 3.2 kcal/mol at the 355

https://dx.doi.org/10.1021/acs.jpca.0c08498
J. Phys. Chem. A 2020, 124, 9166−9176

and 266 nm wavelengths, respectively. These compare to the computed dissociation energies for isomers 1 and 2 of 35−38 and 22−26 kcal/mol, respectively.

The upper limits determined here have implications for the isomer(s) of Ag^+(furan) present in our experiment. The upper limit determined from the 266 nm data is so high as to be consistent with either of the computed values, and it therefore provides no specific insight. However, the limit of 26.3 kcal/mol determined at 355 nm seems to be completely inconsistent with the fragmentation of isomer 1, whose computed dissociation energy is much higher (35−38 kcal/mol). It suggests that our experiment is detecting isomer 2 instead of isomer 1, even though this isomer is much less stable. Interestingly, Yeh and co-workers reported a similar low bond energy (28.1 kcal/mol) in their study of Ag^+(furan), obtained by using a tunable laser and scanning the threshold for the appearance of the furan cation.[22] The threshold measurement of Yeh could be understood if there was *any* population of isomer 2 in their experiment; it could not rule out the presence of another more stable isomer, which would have a threshold overlapping the lower one but beginning at a higher energy. This is true to some extent in our experiment also. A sharp signal for isomer 1 from the dissociation of Ag^+(furan) would have a high energy limit near 0.6 eV, which could be hidden beneath the width of the KER distribution. However, if the width of the KER spectrum for isomer 1 were broad like the others seen here, there would be a signal at lower KER values, i.e., in the center of the image, where there is no signal. Therefore, we cannot rule out the presence of isomer 1, but it seems that either it is not present or it is present, but it has a much sharper KER spectrum than the other ions here. We can conclude that there is a substantial population of isomer 2, which is necessary to explain the position of the high energy edge of the KER spectrum. This result is consistent with that of Yeh and co-workers.[22] The presence of this less stable isomer is somewhat surprising, but not unreasonable. There are several examples of other ions detected recently with infrared spectroscopy where a less stable structure formed in a discharge plasma was kinetically trapped in a local minimum on the global potential surface and survived to be detected.[86] Infrared spectroscopy of the present Ag^+(furan) ions would be useful to determine if both isomers are indeed present and, if so, what the relative concentrations are.

These imaging studies reveal interesting new details on the dynamics of photodissociation and charge transfer in these silver−arene complexes. In each case, dissociative charge transfer was already implicated on the basis of the fragmentation masses from these ions, which each produced the organic cation upon excitation in the near-UV region. However, the imaging experiments show that each of these systems dissociates via an impulsive breakup on the excited state potential, producing significant kinetic energy release. Because of the sensitivity to all fragment ions regardless of their internal states, an overview of the dissociation behavior is provided. Each of these ions dissociates via recoil from an asymmetric structure, resulting in significant excitation of internal rovibrational states, which blurs the image and causes a broad kinetic energy spectrum. The width of this spectrum is narrower for Ag^+(furan) than it is for Ag^+(benzene) or Ag^+(toluene), presumably because the precursor ion has a more symmetric structure (mostly isomer 2 in Figure 4). These fragment ion images generally exhibit a broader KER spectrum with less anisotropy as the excitation energy increases. This can be attributed to factors such as a more energetic "kick" off the excited state surface or a greater change in geometry between the ground and excited states, causing Franck−Condon population of excited vibrations. Another issue likely involved for the benzene and toluene complexes is the possibility of electronic state mixing from ligand-based excited states at nearly the same energies.

A significant issue with these complexes is that the upper limits on the Ag^+−ligand bond energies suggested from the kinetic energy release are generally lower than expected on the basis of theory, and in some cases also lower than the values from previous experiments. Table 1 presents a comparison of the values from theory to those of experiments and previous theory. The Ag^+(benzene) result can be compared to the collision-induced-dissociation (CID) threshold result of Armentrout and co-workers,[33] which was reanalyzed after our initial result came out.[25] The 35.4 ± 2.3 kcal/mol value was higher than our initial imaging upper limit value (32.8 ± 1.5 kcal/mol), and the agreement is worse in the revised value presented here (28.9 ± 3.2 kcal/mol). There are no CID data to our knowledge for Ag^+(toluene), but our derived dissociation energy limit is lower by 4−5 kcal/mol than the values from theory. In the case of Ag^+(furan), our dissociation energy limit (26.3 ± 3.2 kcal/mol) is slightly higher than the value predicted by theory for isomer 2 and agrees within our error bars with the value reported by Yeh and co-workers (28.1 kcal/mol).[22] Thus, we agree reasonably well with theory and previous experiments on Ag^+(furan), but we are systematically lower than other results for the benzene and toluene complexes.

Because of concerns over the Ag^+(benzene) and Ag^+(toluene) dissociation energies, we have carefully considered the possible sources of error in our imaging experiment. If the kinetic energy in the experiment is higher than it should be, this would lead to lower values for the upper limits on the dissociation energies. This could occur if the ions in our experiment were not cooled completely and had unquenched internal energy prior to their photoexcitation. We tested this by using different expansion gases in the cluster source. Helium as an expansion gas gave more kinetic energy, but argon or CO_2 gave comparable results, suggesting that we have cooled the ions as much as is feasible in our experiment. We estimate that our temperatures are 30−50 K, whereas the theory results and the bond energies from Armentrout's work are for 0 K ions. The average internal energy at our estimated temperature can account for about 0.5 kcal/mol, which would shift our values toward higher upper limits on the bond energies. A small amount of multiphoton excitation of the ions with our laser might also shift the image toward higher KER values, but we have done careful power dependence studies to avoid this. A different set of possible issues could affect the CID experiments, especially the large kinetic shifts in thresholds for such large ions, but Armentrout has analyzed these issues and addressed them as much as possible.[41] Finally, our computations and those of others are using DFT methods because of the transition metals, and these methods are recognized to be problematic for thermochemistry. Errors in the range of 5 kcal/mol are not uncommon, and there is no systematic way to improve or extrapolate to more accurate results.[87−91] None of our computations include spin−orbit or relativistic effects which might affect the energetics for silver complexes. Likewise, higher levels of theory such as CCSD(T)

https://dx.doi.org/10.1021/acs.jpca.0c08498
J. Phys. Chem. A 2020, 124, 9166−9176

also have issues with transition metal systems. Therefore, it is not possible at this time to identify the exact source of our thermochemistry discrepancies. Accurate measurements and computations of bonding energetics in such large molecules containing transition metals remain challenging areas for future work.

IV. CONCLUSIONS

$Ag^+(L)$ complexes with benzene, toluene, or furan were found in photodissociation mass spectra to produce organic cation photofragments, indicating that dissociative charge transfer dominates the photodynamics in these systems. Photofragment imaging measurements of the respective organic cation fragments provide evidence for significant release of kinetic energy in each of these systems. The excess energy of photodissociation is partitioned between the kinetic energy of translation and the internal vibrational and rotational degrees of freedom of the molecular cation fragments. The fraction of the energy going into internal excitation increases with the excitation energy. This is attributed to a more energetic kick off the excited state potential, to Franck−Condon effects, or to electronic mixing of the charge transfer state with ligand-based excited states. The maximum KER values for the lowest excitation energies are used in an energetic cycle to determine upper limits on the Ag^+−L dissociation limits. The derived values for Ag^+(benzene) and Ag^+(toluene) are less than those predicted by theory. In the case of the Ag^+(furan) complex, the KER spectrum and the derived dissociation energy suggest that there is significant population for an isomer that is less stable than the global minimum structure by about 12 kcal/mol. Overall, these new data provide new information for charge transfer dynamics on the excited state potential energy surface and new data for the bonding thermochemistry of cation−π complexes.

■ ASSOCIATED CONTENT

Supporting Information

The Supporting Information is available free of charge at https://pubs.acs.org/doi/10.1021/acs.jpca.0c08498.

Full citations for refs 2 and 80; details of DFT computations done in support of the photochemistry presented here, including structures, energetics, and vibrational frequencies for each of the complexes considered; imaging instrument and details about image analysis (PDF)

■ AUTHOR INFORMATION

Corresponding Author

Michael A. Duncan − *Department of Chemistry, University of Georgia, Athens, Georgia 30602, United States;* orcid.org/0000-0003-4836-106X; Email: maduncan@uga.edu

Authors

Brandon M. Rittgers − *Department of Chemistry, University of Georgia, Athens, Georgia 30602, United States*

Daniel Leicht − *Department of Chemistry, University of Georgia, Athens, Georgia 30602, United States*

Complete contact information is available at: https://pubs.acs.org/10.1021/acs.jpca.0c08498

Notes

The authors declare no competing financial interest.

■ ACKNOWLEDGMENTS

We acknowledge generous support for this work from the National Science Foundation through Grant No. CHE-1764111 and from the U.S. Department of Energy through Grant No. DE-SC0018835.

■ REFERENCES

(1) Bagchi, B. Dynamics of Solvation and Charge Transfer Reactions in Dipolar Liquids. *Annu. Rev. Phys. Chem.* **1989**, *40*, 115−141.

(2) Adams, D. M.; Brus, L.; Chidsey, C. E. D.; Creager, S.; Creutz, C.; Kagan, C. R.; Kamat, P. V.; Lieberman, M.; Lindsay, S.; Marcus, R. A.; et al. Charge Transfer on the Nanoscale: Current Status. *J. Phys. Chem. B* **2003**, *107*, 6668−6697.

(3) Ardo, S.; Meyer, G. J. Photodriven Heterogeneous Charge Transfer with Transition-Metal Compounds Anchored to TiO_2 Semiconductor Surfaces. *Chem. Soc. Rev.* **2009**, *38*, 115−164.

(4) Park, H.; Kim, H.-I.; Moon, G.-H.; Choi, W. Photoinduced Charge Transfer Processes in Solar Photocatalysis Based on Modified TiO_2. *Energy Environ. Sci.* **2016**, *9*, 411−433.

(5) Barragan, A. M.; Schulten, K.; Solov'yov, I. A. Mechanism of the Primary Charge Transfer Reaction in the Cytochrome bc_1 Complex. *J. Phys. Chem. B* **2016**, *120*, 11369−11380.

(6) Yam, V. W.-W.; Chan, A. K.-W.; Hong, E. Y.-H. Charge-Transfer Processes in Metal Complexes Enable Luminescence and Memory Functions. *Nature Reviews Chemistry* **2020**, *4*, 528−541.

(7) Hartwig, J. F. *Organotransition Metal Chemistry: From Bonding to Catalysis*; University Science Books: Sausalito, CA, 2010.

(8) Huhey, J. E.; Keiter, E. A.; Keiter, R. L. *Inorganic Chemistry*, 4th ed.; Harper Collins: New York, 1993.

(9) Long, N. J. *Metallocenes*; Blackwell Science: Oxford, U.K., 1998.

(10) Crabtree, R. H. *The Organometallic Chemistry of the Transition Metals*, 5th ed.; John Wiley & Sons: Hoboken, NJ, 2009.

(11) Jarrold, M. F.; Misev, L.; Bowers, M. T. Charge Transfer Half-Collisions: Photodissociation of the $Kr•O_2^+$ Cluster Ion with Resolution of the O_2 Product Vibrational States. *J. Chem. Phys.* **1984**, *81*, 4369−4379.

(12) Illies, J. I.; Jarrold, M. F.; Wagner-Redeker, W.; Bowers, M. T. Photoinduced Intramolecular Charge Transfer: Photodissociation of CO_2^+•Ar Cluster Ions. *J. Am. Chem. Soc.* **1985**, *107*, 2842−2849.

(13) Kim, H.-S.; Kuo, C.-H.; Bowers, M. T. Photon Driven Charge Transfer Half Collisions: The Photodissociation of $CO_2^+•O_2$ Cluster Ions with Resolution of the O_2 Product Vibrational States. *J. Chem. Phys.* **1987**, *87*, 2667−2676.

(14) Willey, K. F.; Cheng, P. Y.; Pearce, K. D.; Duncan, M. A. Photoinitiated Charge Transfer and Dissociation in Mass-Selected Metallo-Organic Complexes. *J. Phys. Chem.* **1990**, *94*, 4769−4772.

(15) Willey, K. F.; Cheng, P. Y.; Bishop, M. B.; Duncan, M. A. Charge-Transfer Photochemistry in Ion−Molecule Cluster Complexes of Silver. *J. Am. Chem. Soc.* **1991**, *113*, 4721−4728.

(16) Willey, K. F.; Yeh, C. S.; Robbins, D. L.; Duncan, M. A. Charge Transfer in the Photodissociation of Metal Ion-Benzene Complexes. *J. Phys. Chem.* **1992**, *96*, 9106−9111.

(17) Jaeger, T. D.; Duncan, M. A. Photodissociation of $M^+(benzene)_x$ Complexes (M = Ti, V, Ni) at 355 nm. *Int. J. Mass Spectrom.* **2005**, *241*, 165−171.

(18) Chen, J.; Wong, T. H.; Cheng, Y. C.; Montgomery, K.; Kleiber, P. D. Photodissociation Spectroscopy and Dynamics of $MgC_2H_4^+$. *J. Chem. Phys.* **1998**, *108*, 2285−2296.

(19) Lu, W.-Y; Kleiber, P. D.; Young, M. A.; Yang, K.-H. Photodissociation Spectroscopy of $Zn^+(C_2H_4)$. *J. Chem. Phys.* **2001**, *115*, 5823−5829.

(20) Yang, Y.-S.; Yeh, C.-S. Photodissociative Charge Transfer in Ag^+-Pyridine Complex. *Chem. Phys. Lett.* **1999**, *305*, 395−400.

(21) Yang, Y.-S.; Hsu, W.-Y.; Lee, H.-F.; Huang, Y.-C.; Yeh, C.-S.; Hu, C.-H. Experimental and Theoretical Studies of Metal Cation-Pyridine Complexes Containing Cu and Ag. *J. Phys. Chem. A* **1999**, *103*, 11287−11292.

(22) Su, P. H.; Yeh, C. S. Photofragmentation of the Ag^+-Furan Complex in the Gas-Phase. *Chem. Phys. Lett.* **2000**, *331*, 420−424.
(23) Su, P. H.; Lin, F. W.; Yeh, C. S. Photodissociation Studies of $M(Furan)^+$ (M = Cu, Ag, and Au) and $Au(C_3H_4)^+$ Complexes. *J. Phys. Chem. A* **2001**, *105*, 9643−9648.
(24) Hsu, H.-C.; Lin, F.-W.; Lai, C.-C.; Su, P.-H.; Yeh, C.-S. Photodissociation and Theoretical Studies of the Au^+-(C_5H_5N) Complex. *New J. Chem.* **2002**, *26*, 481−484.
(25) Maner, J. A.; Mauney, D. T.; Duncan, M. A. Imaging Charge Transfer in a Cation-π System: Velocity-Map Imaging of Ag^+(benzene) Photodissociation. *J. Phys. Chem. Lett.* **2015**, *6*, 4493−4498.
(26) Dougherty, D. A. Cation-π Interactions in Chemistry and Biology: A New View of Benzene, Phe, Tyr, and Trp. *Science* **1996**, *271*, 163−168.
(27) Ma, J. C.; Dougherty, D. A. The Cation-π Interaction. *Chem. Rev.* **1997**, *97*, 1303−1324.
(28) Dougherty, D. A. The Cation-π Interaction. *Acc. Chem. Res.* **2013**, *46*, 885−893.
(29) Mahadevi, A. S.; Sastry, G. N. Cation-π Interaction: Its Role and Relevance in Chemistry, Biology, and Material Science. *Chem. Rev.* **2013**, *113*, 2100−2138.
(30) Hettich, R. L.; Jackson, T. C.; Stanko, E. M.; Freiser, B. S. Gas-Phase Photodissociation of Organometallic Ions. Bond Energy and Structure Determination. *J. Am. Chem. Soc.* **1986**, *108*, 5086−5093.
(31) Eller, K.; Schwarz, H. Organometallic Chemistry in the Gas Phase. *Chem. Rev.* **1991**, *91*, 1121−1177.
(32) Bauschlicher, C. W., Jr.; Partridge, H.; Langhoff, S. R. Theoretical Study of Transition-Metal Ions Bound to Benzene. *J. Phys. Chem.* **1992**, *96*, 3273−3278.
(33) Chen, Y.-M.; Armentrout, P. B. Collision-Induced Dissociation of $Ag(C_6H_6)^+$. *Chem. Phys. Lett.* **1993**, *210*, 123−128.
(34) Afzaal, S.; Freiser, B. S. Gas-phase Photodissociation Study of $Ag(benzene)^+$ and $Ag(toluene)^+$. *Chem. Phys. Lett.* **1994**, *218*, 254−260.
(35) Meyer, F.; Khan, F. A.; Armentrout, P. B. Thermochemistry of Transition Metal Benzene Complexes: Binding Energies of M-$(C_6H_6)_x^+$ (x = 1, 2) for M = Ti to Cu. *J. Am. Chem. Soc.* **1995**, *117*, 9740−9748.
(36) Yasuike, T.; Nakajima, A.; Yabushita, S.; Kaya, K. Why Do Vanadium Atoms Form Multiple-Decker Sandwich Clusters with Benzene Molecules Efficiently? *J. Phys. Chem. A* **1997**, *101*, 5360−5367.
(37) Schroeter, K.; Wesendrup, R.; Schwarz, H. Substituent Effects on the Bond-Dissociation Energies of Cationic Arene-Transition-Metal Complexes. *Eur. J. Org. Chem.* **1998**, *1998*, 565−571.
(38) Dargel, T. K.; Hertwig, R. H.; Koch, W. How Do Coinage Metal Ions Bind to Benzene? *Mol. Phys.* **1999**, *96*, 583−591.
(39) Nakajima, A.; Kaya, K. A Novel Network Structure of Organometallic Clusters in the Gas Phase. *J. Phys. Chem. A* **2000**, *104*, 176−191.
(40) Duncan, M. A. Structures, Energies and Spectroscopy of Gas Phase Transition Metal-Benzene Complexes. *Int. J. Mass Spectrom.* **2008**, *272*, 99−118.
(41) Rodgers, M. T.; Armentrout, P. B. Cationic Noncovalent Interactions: Energetics and Periodic Trends. *Chem. Rev.* **2016**, *116*, 5642−5687.
(42) Reddic, J. E.; Robinson, J. C.; Duncan, M. A. Growth and Photodissociation of Ag_x-C_{60} Cation Complexes. *Chem. Phys. Lett.* **1997**, *279*, 203−208.
(43) Buchanan, J. W.; Grieves, G. A.; Flynn, N. D.; Duncan, M. A. Photodissociation of Silver-Coronene Cluster Cations. *Int. J. Mass Spectrom.* **1999**, *185*−*187*, 617−624.
(44) Yeh, C. S.; Pilgrim, J. S.; Robbins, D. L.; Willey, K. F.; Duncan, M. A. Spectroscopy of Weakly-Bound Magnesium Ion Complexes. *Int. Rev. Phys. Chem.* **1994**, *13*, 231−262.
(45) Lessen, D.; Asher, R. L.; Brucat, P. J. Spectroscopic Characterization of Inductive Binding in Ions. *Int. J. Mass Spectrom. Ion Processes* **1990**, *102*, 331−351.
(46) Sanekata, M.; Misaizu, F.; Fuke, K.; Iwata, S.; Hashimoto, K. Reactions of Singly Charged Alkaline Earth Metal Ions with Water Clusters: Characteristic Size Distribution of Product Ions. *J. Am. Chem. Soc.* **1995**, *117*, 747−754.
(47) Duncan, M. A. Spectroscopy of Metal Ion Complexes: Gas Phase Models for Solvation. *Annu. Rev. Phys. Chem.* **1997**, *48*, 69−93.
(48) Duncan, M. A. Frontiers in the Spectroscopy of Mass-Selected Molecular Ions. *Int. J. Mass Spectrom.* **2000**, *200*, 545−569.
(49) Farrar, J. M. Size-Dependent Reactivity in Open Shell Metal-Ion Polar Solvent Clusters: Spectroscopic Probes of Electronic-Vibration Coupling, Oxidation and Ionization. *Int. Rev. Phys. Chem.* **2003**, *22*, 593−640.
(50) Metz, R. B. Photofragment Spectroscopy of Covalently Bound Transition Metal Complexes: A Window into C-H and C-C Bond Activation by Transition Metal Ions. *Int. Rev. Phys. Chem.* **2004**, *23*, 79−108.
(51) Lias, S. G. Ionization Energy Evaluation. In *NIST Chemistry WebBook, NIST Standard Reference Database Number 69*; Linstrom, P. J., Mallard, W. G., Eds.; National Institute of Standards and Technology: Gaithersburg, MD (accessed 2020-08-04). DOI: 10.18434/T4D303.
(52) Kramida, A., Ralchenko, Yu., Reader, J.; NIST ASD Team *NIST Atomic Spectra Database*, ver. 5.7.1; National Institute of Standards and Technology: Gaithersburg, MD, 2019. https://physics.nist.gov/asd (accessed 2020-08-04).
(53) Parmenter, C. S. Radiative and Non-Radiative Processes in Benzene. *Adv. Chem. Phys.* **2007**, *22*, 365−421.
(54) Hopkins, J. B.; Powers, D. E.; Smalley, R. E. Vibrational Relaxation in Jet-Cooled Alkyl Benzenes. I. Absorption Spectra. *J. Chem. Phys.* **1980**, *72*, 5039−5048.
(55) Christiansen, O.; Jørgensen, P. The Electronic Spectrum of Furan. *J. Am. Chem. Soc.* **1998**, *120*, 3423−3430.
(56) Duncan, M. A. Laser Vaporization Cluster Sources. *Rev. Sci. Instrum.* **2012**, *83*, 041101.
(57) LaiHing, K.; Taylor, T. G.; Cheng, P. Y.; Willey, K. F.; Peschke, M.; Duncan, M. A. Photodissociation in a Reflectron Time-of-Flight Mass Spectrometer: A Novel MS/MS Scheme for High Mass Systems. *Anal. Chem.* **1989**, *61*, 1458−1460.
(58) Cornett, D. S.; Peschke, M.; LaiHing, K.; Cheng, P. Y.; Willey, K. F.; Duncan, M. A. Reflectron Time-of-Flight Mass Spectrometer for Laser Photodissociation. *Rev. Sci. Instrum.* **1992**, *63*, 2177−2186.
(59) *Imaging in Chemical Dynamics*; Suits, A. G., Continetti, R. E., Eds.; ACS Symposium Series 770; American Chemical Society: Washington, DC, 2001.
(60) *Imaging in Molecular Dynamics: Technology and Applications*; Whitaker, B., Ed.; Cambridge University Press: Cambridge, U.K., 2003.
(61) Townsend, D.; Li, W.; Lee, S. K.; Gross, R. L.; Suits, A. G. Universal and State-Resolved Imaging of Chemical Dynamics. *J. Phys. Chem. A* **2005**, *109*, 8661−8674.
(62) Ashfold, M. N. R.; Nahler, N. H.; Orr-Ewing, A. J.; Vieuxmaire, O. P. J.; Toomes, R. L.; Kitsopoulos, T. N.; Garcia, I. A.; Chestakov, D. A.; Wu, S. M.; Parker, D. H. Imaging the Dynamics of Gas Phase Reactions. *Phys. Chem. Chem. Phys.* **2006**, *8*, 26−53.
(63) Eppink, A. T. J. B.; Parker, D. H. Velocity Map Imaging of Ions and Electrons using Electrostatic Lenses: Application in Photoelectron and Photofragment Ion Imaging of Molecular Oxygen. *Rev. Sci. Instrum.* **1997**, *68*, 3477−3484.
(64) Townsend, D.; Minitti, M. P.; Suits, A. G. Direct Current Slice Imaging. *Rev. Sci. Instrum.* **2003**, *74*, 2530−2539.
(65) Li, W.; Chambreau, S. D.; Lahankar, S. A.; Suits, A. G. Megapixel Ion Imaging with Standard Video. *Rev. Sci. Instrum.* **2005**, *76*, 063106. See also: Suits, A. G. NuAcq 0.9 software. http://faculty.missouri.edu/suitsa/NuAcq.html.
(66) Leskiw, B. D.; Kim, M. H.; Hall, G. E.; Suits, A. G. Reflectron Velocity Map Imaging. *Rev. Sci. Instrum.* **2005**, *76*, 104101.
(67) Kim, M. H.; Leskiw, B. D.; Suits, A. G. Vibrationally Mediated Photodissociation of Ethylene Cation by Reflectron Multimass Velocity Map Imaging. *J. Phys. Chem. A* **2005**, *109*, 7839−7842.

https://dx.doi.org/10.1021/acs.jpca.0c08498
J. Phys. Chem. A 2020, 124, 9166−9176

(68) Kim, M. H.; Leskiw, B. D.; Shen, L.; Suits, A. G. Vibrationally Mediated Photodissociation of $C_2H_4^+$. *J. Phys. Chem. A* **2007**, *111*, 7472−7480.
(69) Gichuhi, W. K.; Mebel, A. M.; Suits, A. G. UV Photodissociation of Ethylamine Cation: A Combined Experimental and Theoretical Investigation. *J. Phys. Chem. A* **2010**, *114*, 13296−13302.
(70) Hoshino, H.; Yamakita, Y.; Okutsu, K.; Suzuki, Y.; Saito, M.; Koyasu, K.; Ohshimo, K.; Misaizu, F. Photofragment Imaging from Mass-Selected Ions Using a Reflectron Mass Spectrometer I. Development of an Apparatus and Application to Mg^+-Ar. *Chem. Phys. Lett.* **2015**, *630*, 111−115.
(71) Okutsu, K.; Ohshimo, K.; Hoshino, H.; Koyasu, K.; Misaizu, F. Photofragment Imaging from Mass-Selected Ions Using a Reflectron Mass Spectrometer II. Formation Mechanism of MgF^+ in Photodissociation of Mg^+-FCH_3 Complex. *Chem. Phys. Lett.* **2015**, *630*, 57−61.
(72) Okutsu, K.; Yamazaki, K.; Ohshimo, K.; Misaizu, F. Photofragment Ion Imaging from Mass-Selected Mg^+-$BrCH_3$ Complex: Dissociation Mechanism Following Photoinduced Charge Transfer. *J. Chem. Phys.* **2017**, *146*, 024301.
(73) Okutsu, K.; Nakashima, Y.; Yamazaki, K.; Fujimoto, K.; Nakano, M.; Ohshimo, K.; Misaizu, F. Development of a Linear-Type Double Reflectron for Focused Imaging of Photofragment Ions from Mass-Selected Complex Ions. *Rev. Sci. Instrum.* **2017**, *88*, 053105.
(74) Okutsu, K.; Yamazaki, K.; Nakano, M.; Ohshimo, K.; Misaizu, F. Ion Imaging of MgI^+ Photofragment in Ultraviolet Photodissociation of Mass-Selected Mg^+ICH_3 Complex. *J. Phys. Chem. A* **2018**, *122*, 4948−4953.
(75) Johnston, M. D.; Pearson, W. L., III; Wang, G.; Metz, R. B. A Velocity Map Imaging Mass Spectrometer for Photofragments of Fast Ion Beams. *Rev. Sci. Instrum.* **2018**, *89*, 014102.
(76) Johnston, M. D.; Lockwood, S. P.; Metz, R. B. Photofragment Imaging and Electronic Spectroscopy of Al_2^+. *J. Chem. Phys.* **2018**, *148*, 214308.
(77) Johnston, M. D.; Gentry, M. R.; Metz, R. B. Photofragment Imaging, Spectroscopy, and Theory of MnO^+. *J. Phys. Chem. A* **2018**, *122*, 8047−8053.
(78) Moseley, J. T.; Saxon, R. P.; Huber, B. A.; Cosby, P. C.; Abouaf, R.; Tadjeddine, M. Photofragment Spectroscopy and Potential Curves of Ar_2^+. *J. Chem. Phys.* **1977**, *67*, 1659−1668.
(79) Maner, J. A.; Mauney, D. T.; Duncan, M. A. Velocity Map Ion Imaging Study of Ar_2^+ Photodissociation. *Chem. Phys. Lett.* **2017**, *671*, 182−185.
(80) Frisch, M. J.; Trucks, G. W.; Schlegel, H. B.; Scuseria, G. E.; Robb, M. A.; Cheeseman, J. R.; Scalmani, G.; Barone, V.; Peterson, G. A.; Nakatsuji, H.; et al. *Gaussian 16*; Gaussian, Inc.: Wallingford, CT, 2009.
(81) Ridley, T.; Lawley, K. P.; Al-Kahali, M. H.S.N.; Donovan, R. J. Determination of the First Ionization Energy of Furan (C_4H_4O) from an Extrapolation of Two *n*d Rydberg Series Observed in the Mass-Resolved (2 + 1) Resonance Enhanced Multiphoton Ionization Spectrum. *Chem. Phys. Lett.* **2004**, *390*, 376−379.
(82) Chewter, L. A.; Sander, M.; Müller-Dethlefs, K.; Schlag, E. W. High Resolution Zero Kinetic Energy Photoelectron Spectroscopy of Benzene and Determination of the Ionization Potential. *J. Chem. Phys.* **1987**, *86*, 4737−4744.
(83) Lu, K.-T.; Eiden, G. C.; Weisshaar, J. C. Toluene Cation: Nearly Free Rotation of the Methyl Group. *J. Phys. Chem.* **1992**, *96*, 9742−9748.
(84) Wheeler, S. E. Understanding Substituent Effects in Noncovalent Interactions Involving Aromatic Rings. *Acc. Chem. Res.* **2013**, *46*, 1029−1038.
(85) Wheeler, S. E.; Bloom, J. W. G. Toward a More Complete Understanding of Non-Covalent Interactions Involving Aromatic Rings. *J. Phys. Chem. A* **2014**, *118*, 6133−6147.
(86) Duncan, M. A. Infrared Laser Spectroscopy of Mass-Selected Carbocations. *J. Phys. Chem. A* **2012**, *116*, 11477−11491.
(87) Harvey, J. N. DFT Computation of Relative Spin-State Energetics of Transition Metal Compounds. *Struct. Bonding (Berlin, Ger.)* **2004**, *112*, 151−184.
(88) Cramer, C. J.; Truhlar, D. J. Density Functional Theory for Transition Metals and Transition Metal Chemistry. *Phys. Chem. Chem. Phys.* **2009**, *11*, 10757−10816.
(89) Cohen, A. J.; Mori-Sanchez, P.; Yang, W. Challenges for Density Functional Theory. *Chem. Rev.* **2012**, *112*, 289−320.
(90) Shil, S.; Bhattacharya, D.; Sarkar, S.; Misra, A. Performance of the Widely Used Minnesota Density Functionals for the Prediction of Heat of Formations, Ionization Potentials of Some Benchmarked First Row Transition Metal Complexes. *J. Phys. Chem. A* **2013**, *117*, 4945−4955.
(91) Moltved, K. A.; Kepp, K. P. Chemical Bond Energies of 3d Transition Metals Studied by Density Functional Theory. *J. Chem. Theory Comput.* **2018**, *14*, 3479−3492.

https://dx.doi.org/10.1021/acs.jpca.0c08498
J. Phys. Chem. A 2020, 124, 9166−9176